Electronic supplementary information

for

Heteroatoms Constructed Covalent Organic Frameworks for Oxygen Electrocatalysis and Rechargeable Zinc-Air Battery

Anup Kumar Pradhan,[a] Bhushan Kishor Nandre,[a] Pandiyan Sivasakthi,[a] Sayan Halder,[a] Sasanka Dalapati,[b] Asim Bhaumik,[c] Pralok K. Samanta,[a,] Chanchal Chakraborty,[a,]**

[a] Department of Chemistry, Birla Institute of Technology & Science (BITS) Pilani, Hyderabad Campus, Jawaharnagar, Samirpet, Hyderabad, Telangana 500078, India

[b] Department of Materials Science, School of Technology, Central University of Tamil Nadu (CUTN), Thiruvarur -610005, Tamil Nadu, India.

[c] School of Materials Sciences, Indian Association for the Cultivation of Science (IACS), 2A & 2B Raja S. C. Mallick Road, Jadavpur, Kolkata – 700032, West Bengal, India.

Corresponding Authors: Dr. Chanchal Chakraborty (Email: chanchal@hyderabad.bits-pilani.ac.in)

Dr. Pralok K. Samanta (Email: pralokkumar.samanta@hyderabad.bits-pilani.ac.in)

Materials and methods

The chemicals used in the study including Benzo[1,2-b:3,4-b':5,6-b"]trithiophene-2,5,8-tricarbaldehyde (BTTh), tris (4-formyl phenyl) amine (TFPA) and 2,4,6-tris-(4-aminophenyl)-1,3,5-triazine (TAPA), were purchased from BLD Pharma, and other solvents such as methanol (MeOH), tetrahydrofuran (THF), acetonitrile (ACN), dimethyl formamide (DMF), butanol (n-

BuOH), *o*-dichlorobenzene (o-DCB) and acetic acid (AcOH) were acquired from Sisco Research Laboratories (SRL) India Pvt. Ltd.

Synthesis of BTTh-TZ-COF

The synthesis of **BTTh-TZ-COF** was carried out following a previously reported procedure, as shown in Scheme 1. In a typical process, 40 mg (0.12 mmol) of BTTh and 42 mg (0.12 mmol) of TAPA were dissolved in a mixture of o-dichlorobenzene and 1-butanol in a 10 mL Schlenk sealed tube. This solution was sonicated for approximately 30 minutes to achieve a uniform dispersion. Following this, 0.3 mL of 6 M acetic acid was added dropwise, and the solution was sonicated for an additional 5 minutes, resulting in a dark yellow solution. The mixture was then degassed by performing three freeze-pump-thaw cycles. It was first frozen using liquid nitrogen at –78 °C and then vacuum-sealed. The sealed solution was heated at 120 °C for 72 hours. When the solution temperature reached room temperature, the solid precipitate was filtered and thoroughly washed multiple times with water, methanol, ethanol, and tetrahydrofuran. The material was subjected to Soxhlet extraction using DMF to remove any residual starting materials and oligomers. Finally, the yellowish solid was collected and dried overnight at 120 °C under vacuum, yielding the target product with an 82% yield.

Synthesis of TPA-TZ-COF

TAPA (80 mg; 0.24 mmol), TFPA (86 mg; 0.24 mmol), 6 M acetic acid (0.02 mL), o-dichlorobenzene (1.5 mL), and 1-butanol (1.5 mL) were added to a 10 mL Schlenk sealed tube and heated at 120 °C for 72 hours. The remaining steps followed the same procedure as that used for the synthesis of **TPA-TZ-COF**. The final product obtained was referred to as **TPA-TZ-COF** (110 mg),

Preparation of electrodes for electrocatalysis

The catalyst was prepared by adding 2 mg of the COF-based materials in a 4:1 ratio of ethanol and water solution to study the electrocatalytic behavior. We also used the activated carbon (2 mg) to increase the conductivity of the catalyst. A portion of 10 μL of Nafion was used as a binder in the catalyst mixture. The resulting dispersion was then sonicated for 1 h to ensure uniformity. For ORR measurements, 5 μL of the catalyst ink obtained from the homogeneous mixture was drop-cast onto the surface of a glassy carbon electrode (GCE) Rotating Ring Disk Electrode (RRDE) with an area of 0.2 cm^2. The electrode was then dried in a vacuum oven for 24 hours and used for electrocatalytic studies. For the OER experiment, 10 μL of catalyst was coated on a 0.8 × 0.8 cm^2 area of 2 × 1 cm^2 nickel foil.

Rotating disk electrode (RDE) measurements:

Electrode materials were cathodically scanned in RDE measurements, from 0.2 to -0.8 V (vs. SCE) in 0.1M KOH at a scan rate of 10 mV s^{-1}, having different rotation speeds from 400 to 2000 rpm. Koutecky-Levich (K-L) plots are derived from CLSV data measured. The number of electrons transferred was calculated based on the following K-L equation,

$$\frac{1}{j} = \frac{1}{jl} + \frac{1}{jk} = \frac{1}{B\omega^{1/2}} + \frac{1}{jk}$$

$$B = 0.2nFC_0(D_0)^{2/3}\, v^{-1/6}$$

Where, j = current density, j_l & j_k = diffusion- and kinetic-limiting current densities, ω = angular velocity, F = Faraday constant, C_0 = bulk concentration of O_2, D_0 = diffusion coefficient of O_2 in electrolyte, N = number of electrons transferred, v = kinematic viscosity of the electrolyte.

Rotating ring-disk electrode (RRDE) measurements:

In RRDE measurements, the electrode material was cathodically scanned from 0.2 to -0.8 V (vs. SCE) at a scan rate of 10 mV /s in 0.1M KOH, keeping the ring potential constant at 1.5 V

vs. RHE. The number of electrons transferred (n) was calculated by using the following equations:

$$\mathbf{n = 4 \times \frac{I_d}{I_d + I_r/N}}$$

Where, I_d = disk current, I_r = ring current, N = current collection efficiency of the Pt ring (37%).

Calculation of the Battery Performances:

The specific capacity of the assembled zinc-air batteries was calculated from the equation below:

Specific capacity = $\boldsymbol{I \times t/m_{Zn}}$

The energy can be calculated from the equation below:

Energy density = $\boldsymbol{I \times t \times V/m_{Zn}}$

Where *I* denotes current, t denotes the service hours, V denotes the average discharge voltage, and m_{Zn} denotes the weight of consumed zinc.

Modeling of COFs:

The unit cell of the extended COFs structures was built using Materials Studio software, and geometry optimization was performed by the DFTB (density functional tight binding) method with self-consistent charge (SCC) and dispersion correction functions. The optimization parameters were selected from the Slater-Koster library (*mio*, 1×1×1, *k-point* set - medium). The optimized unit cell was then used for Pawley refinement to verify the powder XRD data. The unit cell was optimized, and simulated XRD, reflection planes, and lattice parameters were evaluated.[2-3]

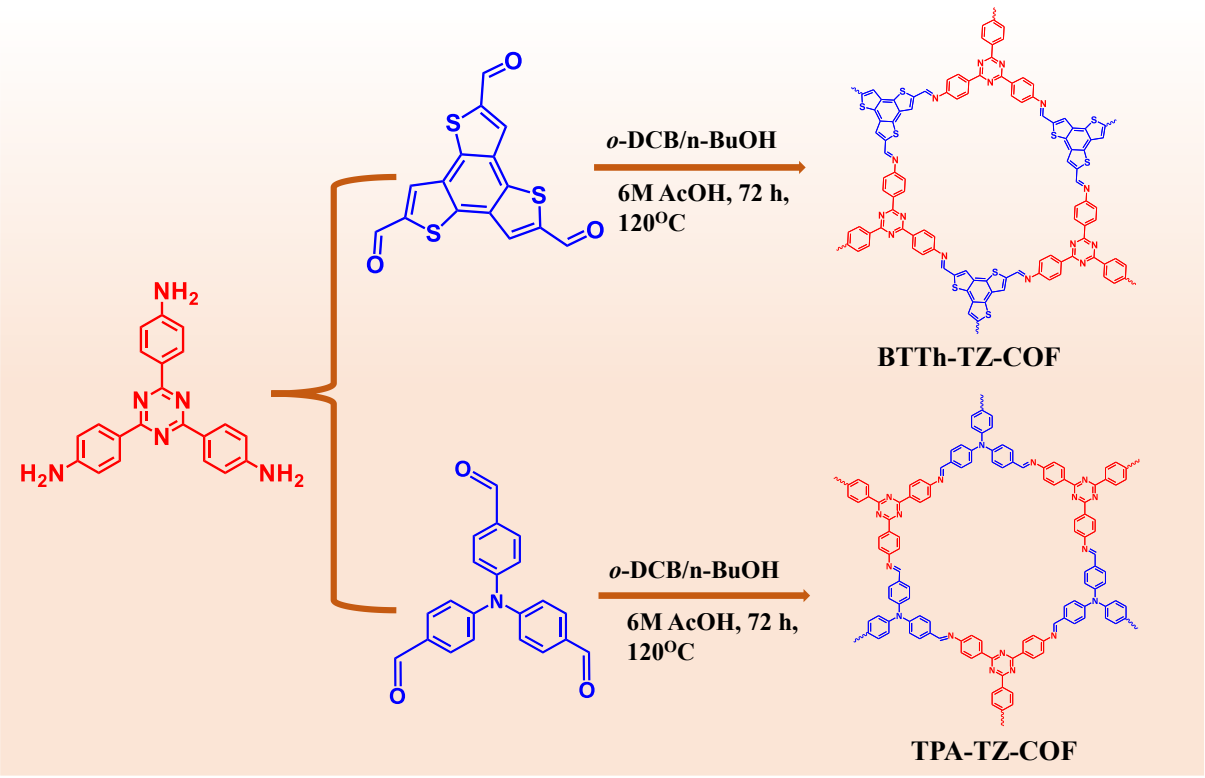

Scheme S1. Schematic diagram of the synthesis of **BTTh-TZ-COF** and **TPA-TZ-COF**.

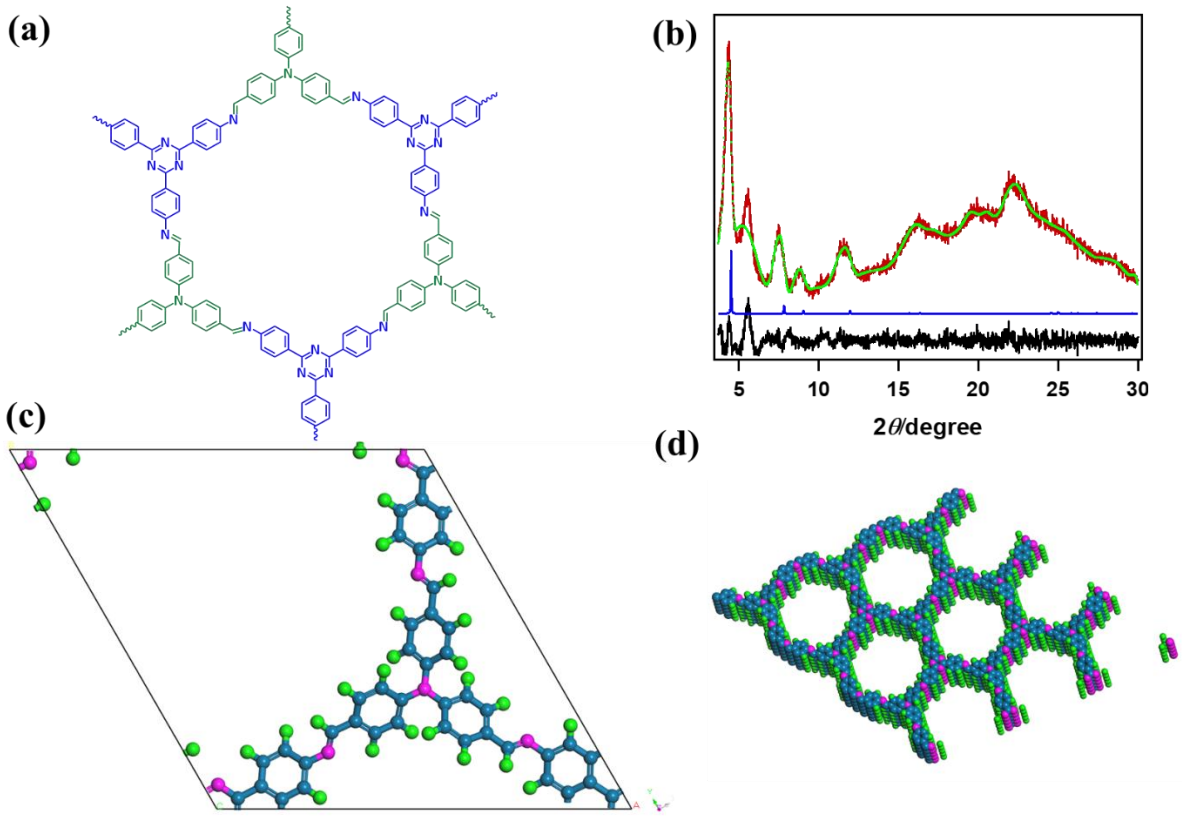

Fig. S1. (a) Chemical structure of the **TPA-TZ-COF**. (b) Powder X-ray diffraction data of **TPA-TZ-COF**. Observed diffraction, Pawley refined data, the difference between experiment and Pawley refined data, and theoretical diffraction of the 2D COFs have been presented with red, green, black, and blue color graphs, respectively. (c) Unit cells of the **TPA-TZ-COF**. Color codes: C-steel blue, H-green, S-orange, N-magenta. **(d)** An extended 2D stacked structure (3 × 3 × 5 super cell) of the **TPA-TZ-COF**. Color codes: C-steel blue, H-green, S-orange, N-magenta.

Table S1. Atomistic coordinates for the **TPA-TZ-COF** after Pawley refinement.

Unit cell: a = b = 22.58 Å, c = 3.62 Å, α = β = 90°, and γ = 120°, Space group P_3			
Atom	**X**	**Y**	**Z**
C	0.59666	0.304	0.07447
C	0.55542	0.24121	-0.08018
C	0.48694	0.21213	-0.07327
C	0.45608	0.24464	0.08312
C	0.49695	0.30753	0.23346
C	0.56549	0.33637	0.23185
C	0.38387	0.21406	0.09041
N	0.34668	0.15736	-0.05504
N	0.03671	0.06755	-0.10509
C	-0.02991	0.03561	-0.10473
C	0.1384	0.06324	-0.09746
C	0.17059	0.0278	-0.00702
C	0.23929	0.05926	0.00697
C	0.27763	0.12765	-0.06365
C	0.24574	0.16318	-0.16177
C	0.17696	0.13111	-0.17709
H	0.57687	0.21443	-0.21264
H	0.45632	0.16338	-0.19701
H	0.4747	0.33418	0.36142
H	0.59481	0.38462	0.36097
H	0.36329	0.2421	0.23375
H	0.14077	-0.02525	0.0552
H	0.26399	0.03155	0.08434
H	0.27508	0.21593	-0.23173
H	0.15224	0.1589	-0.25359
N	0.66667	0.33333	1.07242

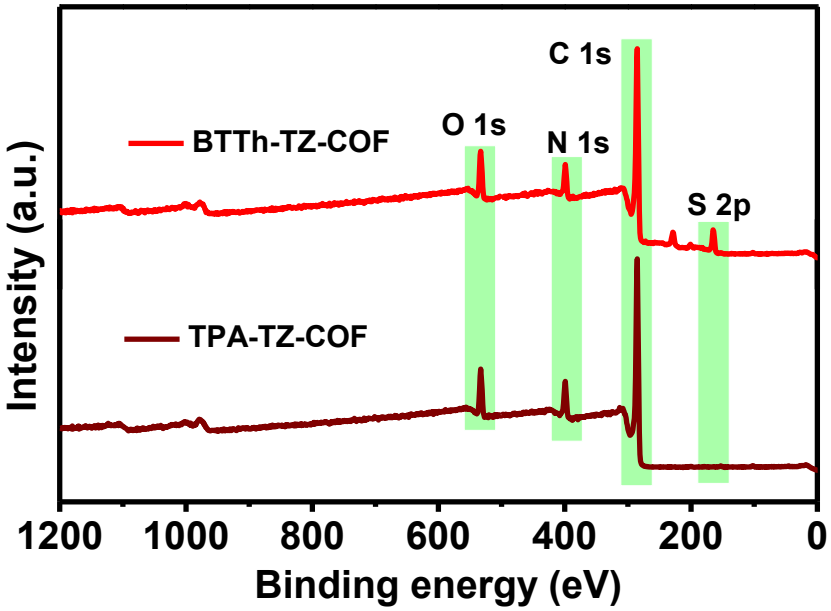

Fig. S2 XPS survey spectra of **BTTh-TZ-COF** and **TPA-TZ-COF**.

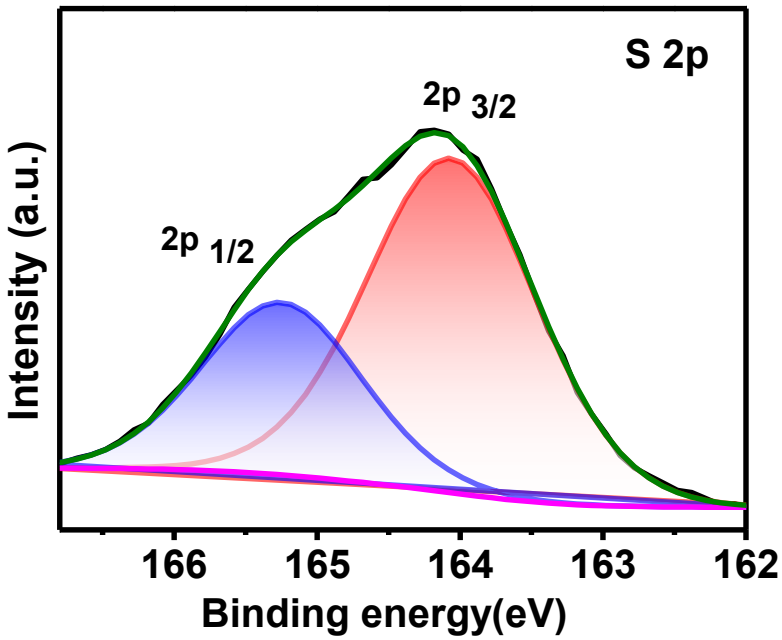

Fig. S3. Core-level XPS spectra of S 2p in **BTTh-TZ-COF**.

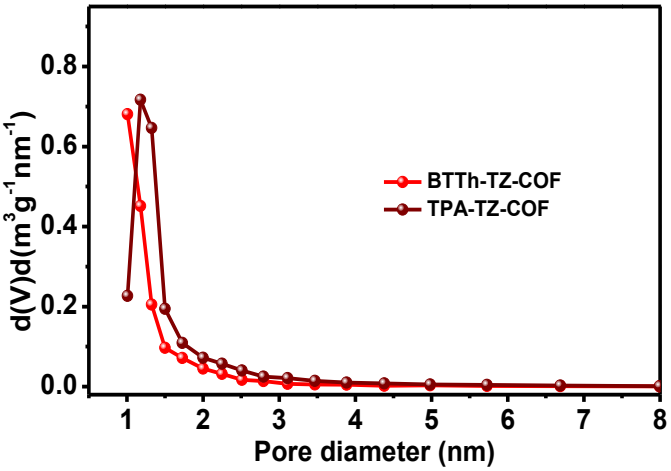

Fig. S4 Pore size distribution plot of **BTTh-TZ-COF** and **TPA-TZ-COF**.

Table S2. Summarization of all the obtained BET parameters.

Catalysts	**Surface Area (m^2g^{-1})**	**Pore Diameter (nm)**	**Total Pore Volume (cm^3/g)**	**Theoretical Pore Size (nm)**
BTTh-TZ-COF	820	1.17	0.25	1.75
TPA-TZ-COF	1136	1.18	0.41	1.94

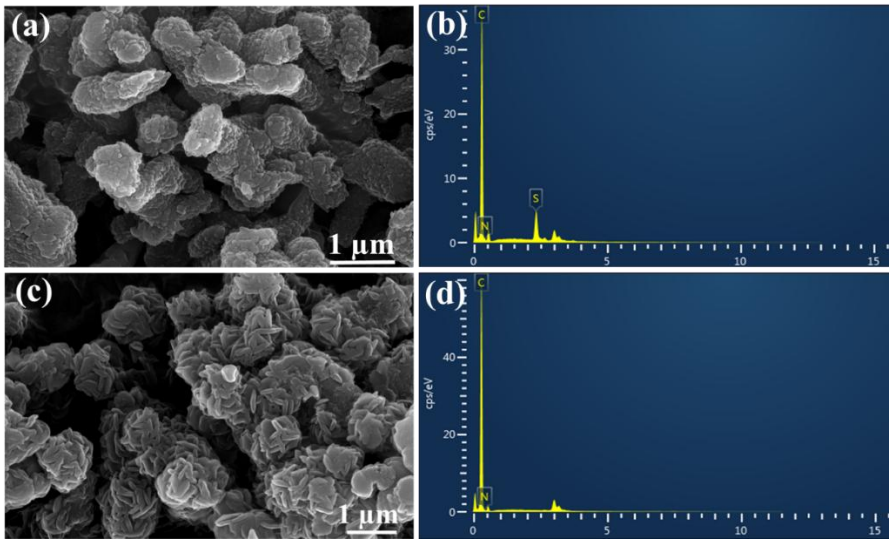

Fig. S5. (a) FE-SEM image and (b) corresponding EDX spectra of **BTTh-TZ-COF**. (c) FE-SEM image and (d) corresponding EDX spectra of **TPA-TZ-COF.**

In Fig. S5a, **BTTh-TZ-COF** reveals a spherical aggregated morphology having a diameter between 100 and 200 nm. The aggregated morphology disclosed the strong interlayer π–π stacking between the COF layers. The energy-dispersive X-ray (EDX) spectroscopy of **BTTh-TZ-COF** in Fig. S5b reveals the presence of all required elements like C, N, and S in the structure. The SEM image of **TPA-TZ-COF** (Fig. S5c) shows a self-assembled, aggregated morphology arising from interlayer π–π stacking within its 2D nanosheet structures. The EDX spectroscopy of **TPA-TZ-COF** in Fig. S5d reveals the presence of homogeneously distributed C and N as the main constituent elements.

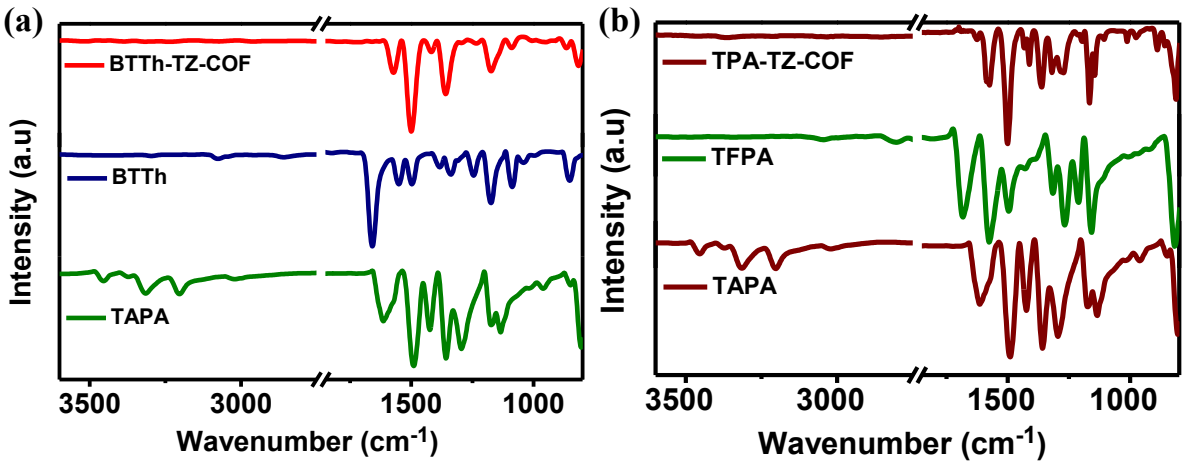

Fig. S6 FT-IR spectra of (a) **BTTh-TZ-COF**, (b) **TPA-TZ-COF** with their precursors.

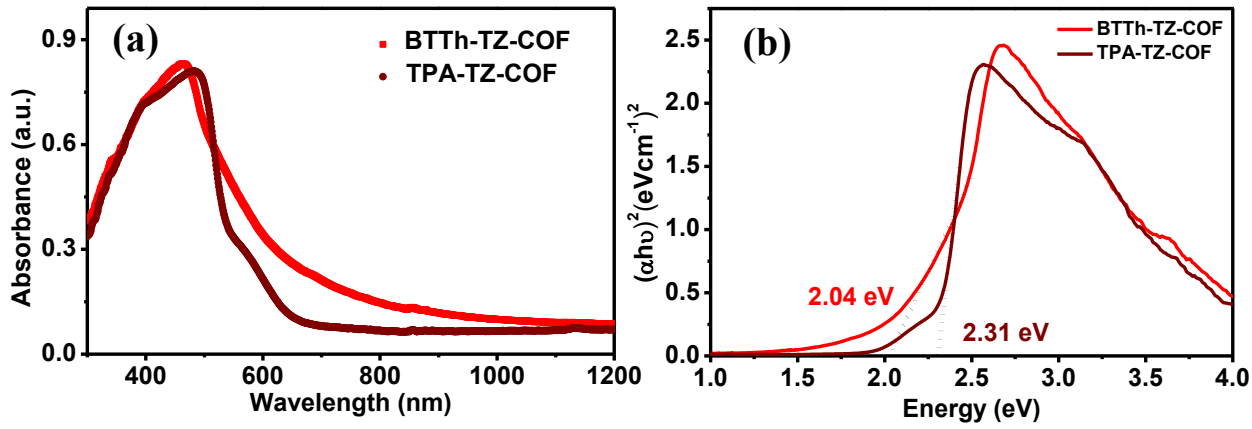

Fig. S7 (a) Solid state UV-Vis spectra, and (b) optical band gap calculation of **BTTh-TZ-COF** and **TPA-TZ-COF.**

"Calculation of HOMO and LUMO positions:

Both the highest occupied molecular orbital (HOMO) and the lowest unoccupied molecular orbital (LUMO) energy levels of BTTh-TZ-COF and TPA-TZ-COF were determined directly from cyclic voltammetry measurement performed using a typical three-electrode electrode-based electrochemical set-up, considering catalyst-coated ITO, Ag/AgCl-sat. KCl and a Pt wire as the working and reference electrodes, and counter electrode, respectively, in 0.1 M $LiClO_4$/acetonitrile electrolyte at a scan rate of 50 mV/s. The HOMO and LUMO positions are directly measured by extracting the onset oxidation (E_{Ox}^{Onset}) and onset reduction (E_{Red}^{Onset}) potentials, respectively, as represented in **Fig. S8**.

The onset potentials were obtained by extrapolating the tangent of the sudden rising current to the baseline. All electrochemical potentials were calibrated using ferrocene/ferrocenium (Fc/Fc^+) as an internal reference standard.

The energy levels are calculated using the following equations:

$E_{HOMO\ (BTTh\text{-}TZ\text{-}COF)} = -(E_{Ox}^{Onset} - 0.49 + 4.8)\ eV = -[0.76 - 0.49 + 4.8]\ eV = -5.07\ eV$

$E_{HOMO\ (TPA\text{-}TZ\text{-}COF)} = -(E_{Ox}^{Onset} - 0.49 + 4.8)\ eV = -[0.83 - 0.49 + 4.8]\ eV = -5.14\ eV$

$E_{LUMO\ (BTTh\text{-}TZ\text{-}COF)} = -(E_{Red}^{Onset} - 0.49 + 4.8)\ eV = -[(-1.39) - 0.49 + 4.8]\ eV = -2.92\ eV$

$E_{LUMO\ (TPA\text{-}TZ\text{-}COF)} = -(E_{Red}^{Onset} - 0.49 + 4.8)\ eV = -[-1.41\ -0.49 + 4.8]\ eV = -2.9\ eV$

Bandgap, $E_g = E_{LUMO} - E_{HOMO}$

E_g (BTTh-TZ-COF) = 2.15 eV

E_g (TPA-TZ-COF) = 2.24 eV

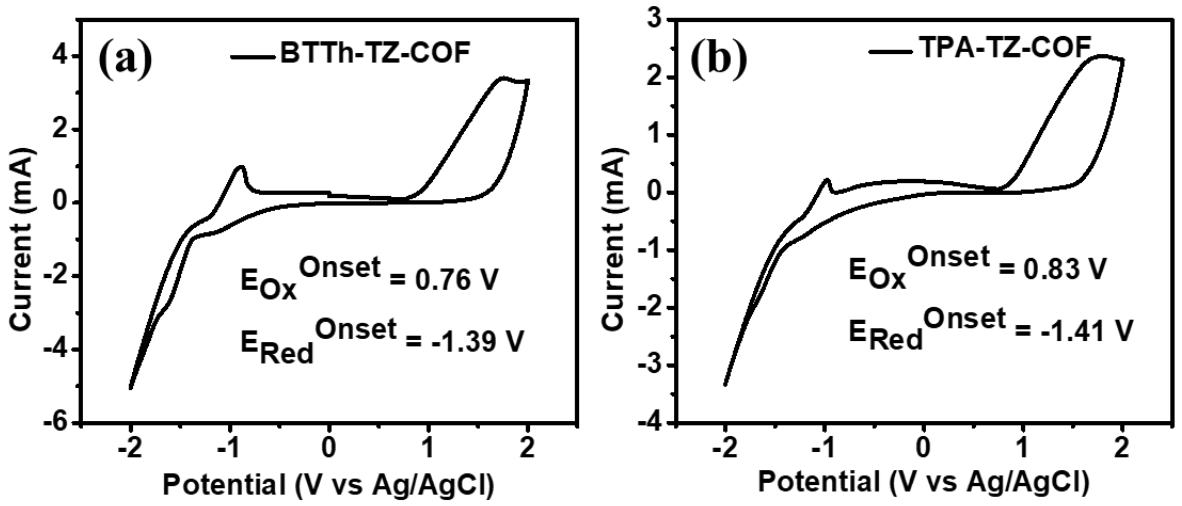

Fig. S8 CV plot to calculate the HOMO and LUMO positions of (a) **BTTh-TZ-COF,** (b) **TPA-TZ-COF**

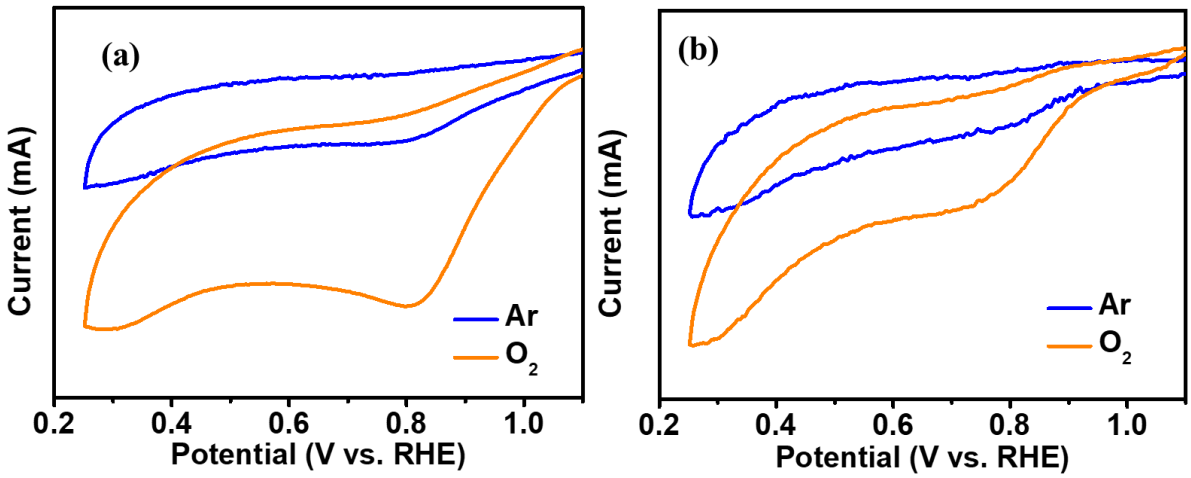

Fig. S9 CV study for oxygen reduction for (a) **BTTh-TZ-COF** (b) **TPA-TZ-COF** catalyst in presence of Argon and O_2 saturated condition in 0.1 M KOH electrolyte.

Table S3. ORR performance parameter comparison table to compare **BTTh-TZ-COF** with other reported COF materials

Sample	E_{onset} (V) vs. RHE	$E_{1/2}$ (V) vs. RHE	References
Im-PY-BPY-COF	0.9	0.8	4
PTCOF	0.8	0.7	5
JUC-610-CONs	0.83	0.72	6
JUC-528	0.83	0.7	7
BUCT-COF	0.82	0.72	8
COF-β	0.87	0.76	9
CC-3	0.92	0.828	10
3D-Tr-COF	0.938	0.833	11
JUC-650	0.9	0.72	12
DAF-COF	0.89	0.74	13
Azo-COF	0.88	0.68	14
Pt/C	1.01	0.90	This work
TPA-TZ-COF	**0.83**	**0.77**	**This work**
BTTh-TZ-COF	**0.92**	**0.82**	**This work**

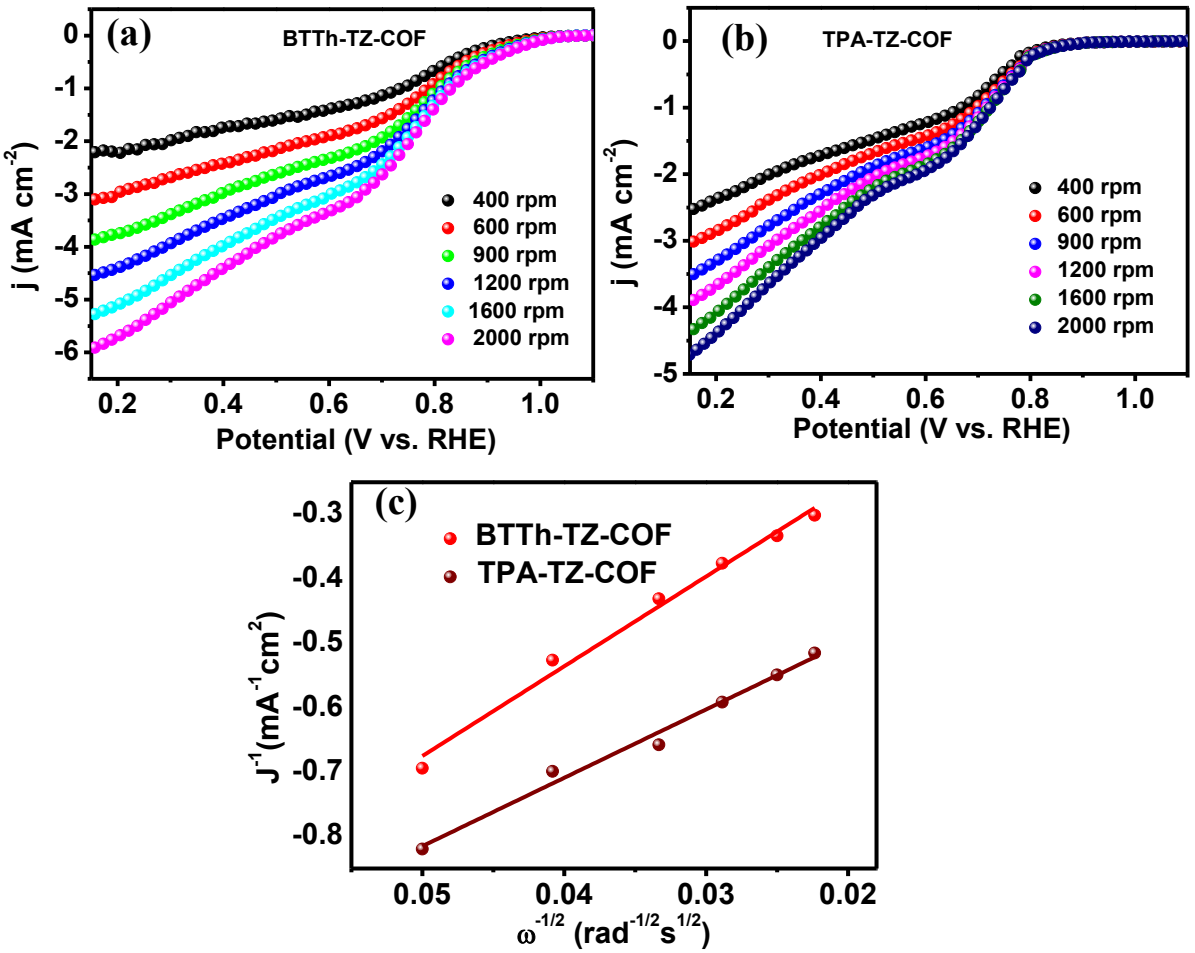

Fig. S10 CLSV curves at different rpm for (a) **BTTh-TZ-COF** and (b) **TPA-TZ-COF**. (c) Derived K-L plot of **BTTh-TZ-COF** and **TPA-TZ-COF**.

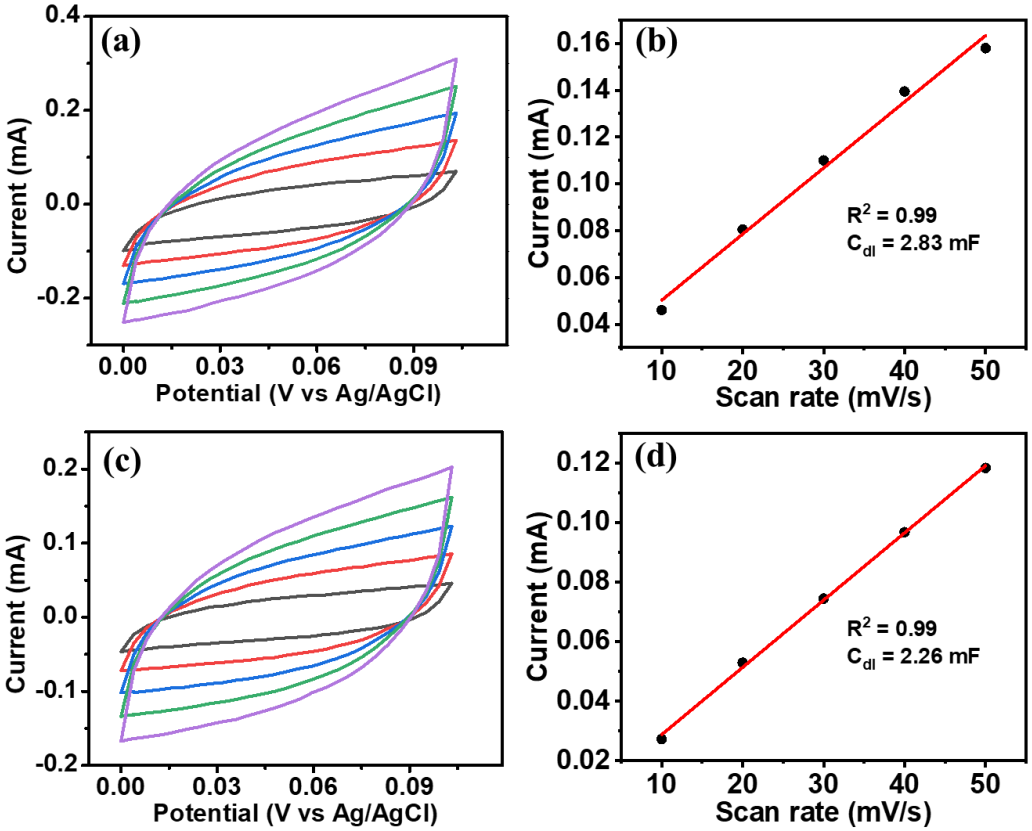

Fig. S11 (a) CV curves in the non-faradic region for **BTTh-TZ-COF** at different scan rates, and (b) derived C_{dl} plot of **BTTh-TZ-COF**. (c) CV curves in the non-faradic region for **TPA-TZ-COF** at different scan rates, and (d) derived C_{dl} plot of **TPA-TZ-COF**.

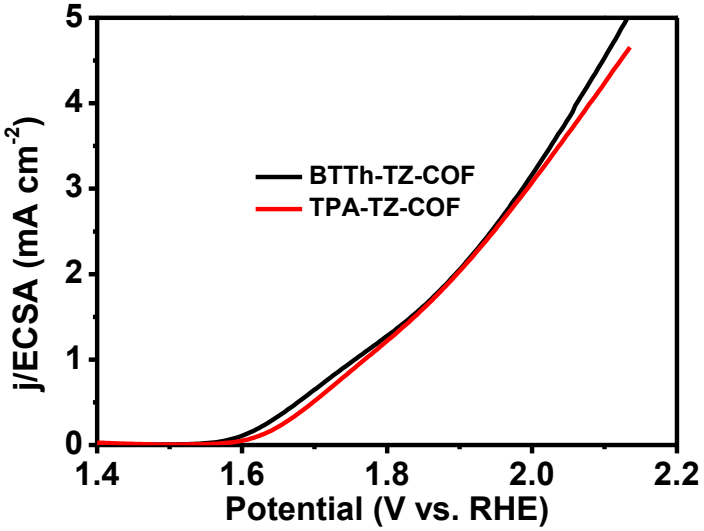

Fig. S12 ECSA homogenized LSV curves of BTTh-TZ-COF and TPA-TZ-COF.

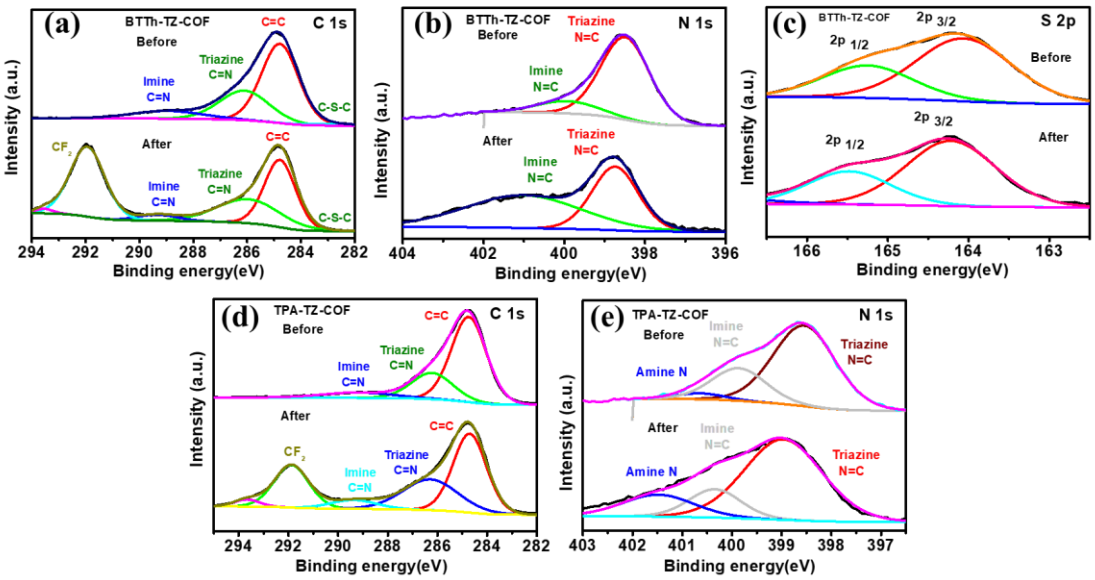

Fig. S13 Post-OER XPS spectra of (**a**) C 1s spectra, (b) N 1s spectra, (c) S 2p spectra in BTTh-TZ-COF, and (d) C 1s and (e) N 1s in TPA-TZ-COF.

Theoretical Study and Computational Methodology:

All periodic density functional theory (DFT) calculations were carried out using the Vienna Ab initio Simulation Package (VASP).[15] A plane-wave basis set with an energy cutoff of 400 eV was employed. Ion–electron interactions were described using projector-augmented wave (PAW) pseudopotentials. The exchange–correlation effects were treated with the Perdew–Burke–Ernzerhof (PBE) functional within the generalized gradient approximation (GGA).[16,17] We also tested our results using the B3LYP functional. The van der Waals (vdW) interactions between the COF layer and OER/ORR organic molecules were predicted using the DFT-D3 method with Becke–Johnson (BJ) damping. The Brillouin zone integration was performed using a 2 × 2 × 1 Monkhorst–Pack k-point grid.[18] Structural optimizations were conducted with the conjugate gradient method until the total energy converged to within 1×10^{-6} eV. During relaxation, all atoms in both the COF and the adsorbed molecules were allowed to move freely in the X, Y, and Z directions.

Table S4. Different adsorption sites of the two COFs (See Fig. S14) and corresponding total energy in eV using the PBE exchange-correlation functional.

BTTh-TZ-COF	Adsorption site	**C1**	C2	C3	C4	C5	C6	C7	C8	N1	S1
	Adsorption of OH	**-460.33**	-459.65	-459.91	-459.27	- 459.71	-456.48	-459.42	-455.89	-459.93	- 456.33
	Adsorption of O	**-456.16**	**-456.19**	-455.37	-455.53	-455.88	-453.67	-455.50	-455.80	-455.37	**-456.18**
	Adsorption of OOH	**-464.505**	-464.49	-463.88	-463.94	- 463.95	-463.90	-463.90	-463.79	-463.77	- 463.93
TPA-TZ-COF	Adsorption site	C1	C2	C3	**C4**	C5	C6	C7	C8	C9	N1
	Adsorption of OH	-542.50	-542.49	-542.25	**-542.65**	-542.12	-542.63	-542.59	-542.18	-541.48	-541.67
	Adsorption of O	-538.79	-538.79	-538.42	**-538.30**	**-538.31**	-538.70	**-539.25**	-538.25	**-540.13**	**-539.08**
	Adsorption of OOH	-546.79	-546.78	**-546.84**	**-546.83**	Not-stable	-546.54	-546.66	-546.69	-546.67	Not-stable

Table S5. Free-energy change (ΔG in eV) for OER steps of each site (See Fig. S14) of the two COFs using the PBE exchange-correlation functional.

BTTh-TZ-COF					**TPA-TZ-COF**				
	$\Delta G_{*\rightarrow *OH}$	**$\Delta G_{*OH\rightarrow *O}$**	**$\Delta G_{*O\rightarrow *OOH}$**	**$\Delta G_{*OOH\rightarrow O_2}$**		**$\Delta G_{*\rightarrow *OH}$**	**$\Delta G_{*OH\rightarrow *O}$**	**$\Delta G_{*O\rightarrow *OOH}$**	**$\Delta G_{*OOH\rightarrow O_2}$**
C1	**1.74**	**1.07**	**2.79**	**1.18**	C1	2.41	0.62	3.13	0.63
C2	2.41	0.37	2.83	1.17	C2	2.43	0.60	3.14	0.62
C3	2.15	1.44	2.62	0.56	C3	2.66	0.74	2.71	0.68
C4	2.79	0.65	2.72	0.61	**C4**	**2.26**	**1.26**	**2.51**	**0.76**
C5	2.35	0.73	3.06	0.63	C5	2.79	0.71	--	--
C6	5.58	-0.28	0.91	0.57	C6	2.28	0.83	3.29	0.37
C7	2.65	0.82	2.74	0.58	C7	2.32	0.24	3.72	0.50
C8	6.18	-3.01	3.15	0.47	C8	2.73	0.83	2.69	0.53
N1	2.14	1.46	2.73	0.45	C9	3.43	-1.74	4.59	0.50
S1	5.73	-2.94	3.37	0.61	N1	3.24	-0.50	--	--

Note: There are six sites (C1, C2, C3, C4, C7 and N1) with highest energy barrier (~2.79 eV) for BTTh-TZ-COF. There are three sites (C3, C4, and C8) with highest energy barrier (~2.51 eV) for TPA-TZ-COF.

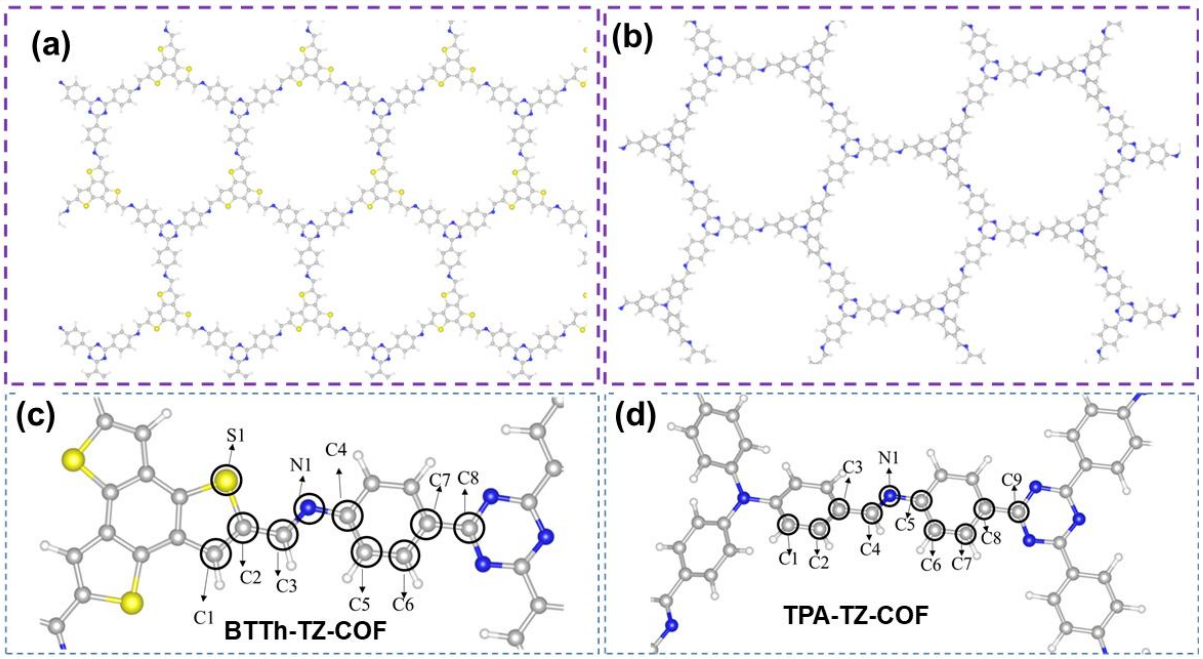

Fig. S14. Structures of (a) **BTTh-TZ-COF** and (b) **TPA-TZ-COF**. Different adsorption sites in (c) **BTTh-TZ-COF** and (d) **TPA-TZ-COF** structures.

Oxygen Evaluation Reaction Mechanism

For OER in an alkaline medium, the overall reaction is shown in Fig. S13.

$$* + OH^- \rightarrow *OH + e^- \quad (1)$$

$$*OH + OH^- \rightarrow *O + H_2O + e^- \quad (2)$$

$$*O + OH^- \rightarrow *OOH + e^- \quad (3)$$

$$*OOH + OH^- \rightarrow * + H_2O + O_2\ e^- \quad (4)$$

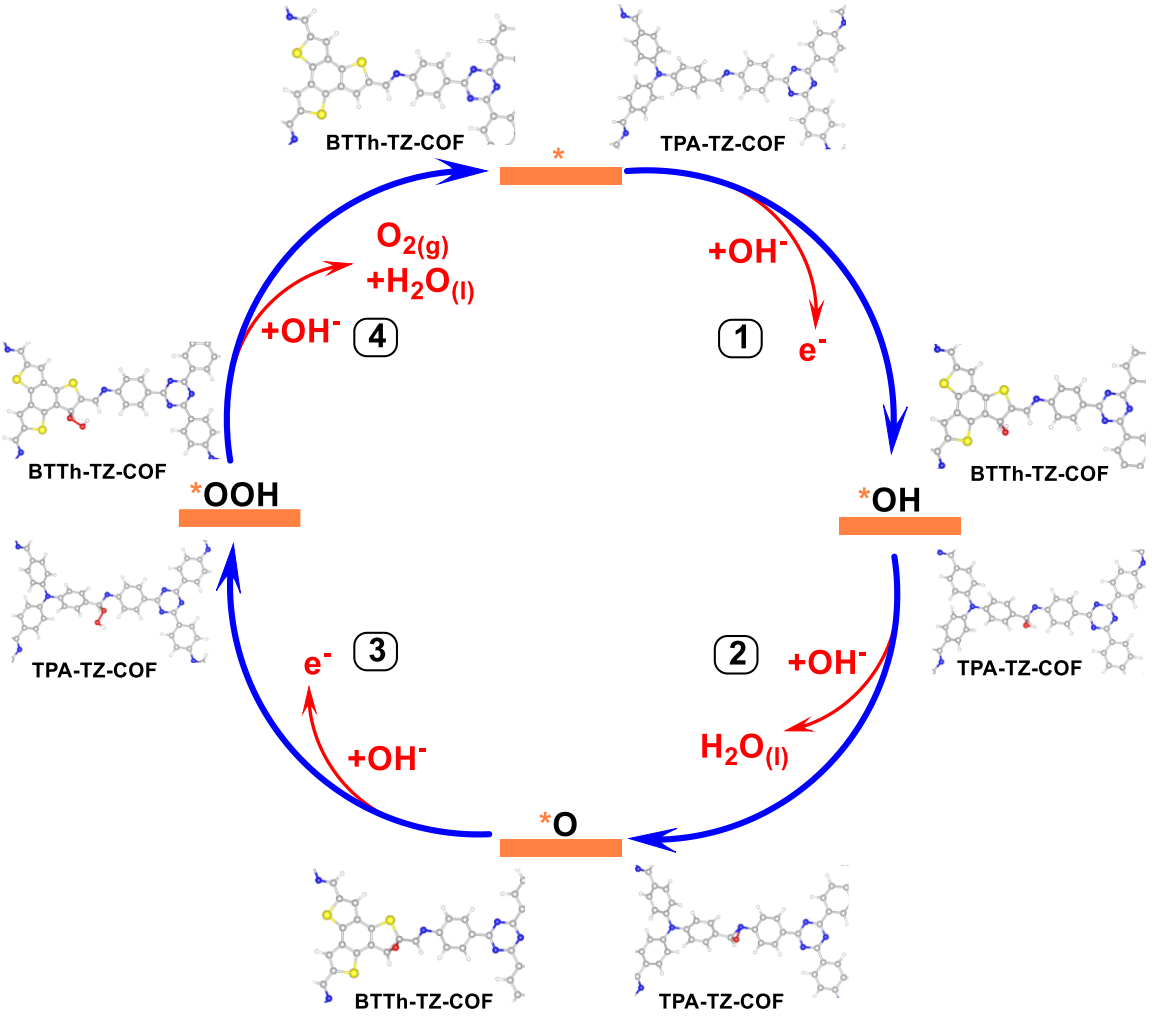

Fig. S15 Oxygen Evaluation Reaction Mechanism on **BTTh-TZ-COF** and **TPA-TZ-COF**.

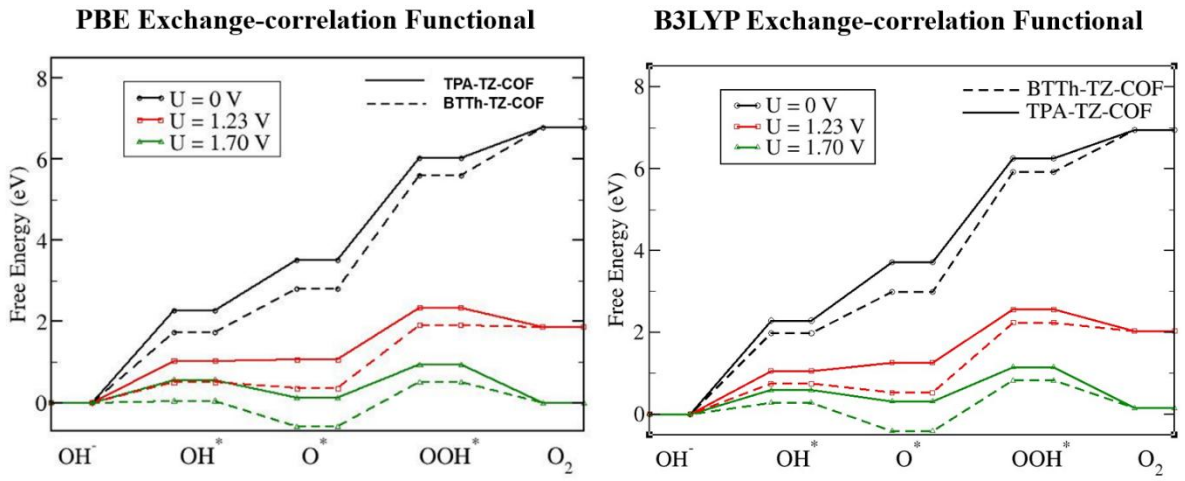

Fig. S16 The free energy diagram of the OER for **TPA-TZ-COF** (solid line) and **BTTh-TZ-COF** (dotted line) on the COF's surface at potentials of U = 0 V (black line), 1.23 V (red line), and 1.70 V (green line) (vs RHE) using PBE and B3LYP exchange-correlation functional.

Oxygen Reduction Reaction Mechanism:

The electrocatalytic ORR properties of these COFs were investigated through the computational hydrogen electrode (CHE) approach introduced by Nørskov and co-workers.[19]

For four-electron ORR in an alkaline medium, the overall reaction is shown in Fig. S13.[19,20]

$$* + O_{2(g)} \rightarrow *O_2 \quad (5)$$

$$*O_2 + H_2O_{(l)} + e^- \rightarrow *OOH + OH^- \quad (6)$$

$$*OOH + e^- \rightarrow *O + OH^- \quad (7)$$

$$*O + H_2O_{(l)} + e^- \rightarrow *OH + OH^- \quad (8)$$

$$*OH + e^- \rightarrow OH^- + * \quad (9)$$

For two-electron ORR in an alkaline medium, the overall reaction is shown in Fig. S15 and Eqn. 5, 6, and 7a).

$$*OOH + e^- \rightarrow * + OOH^- \quad (7a)$$

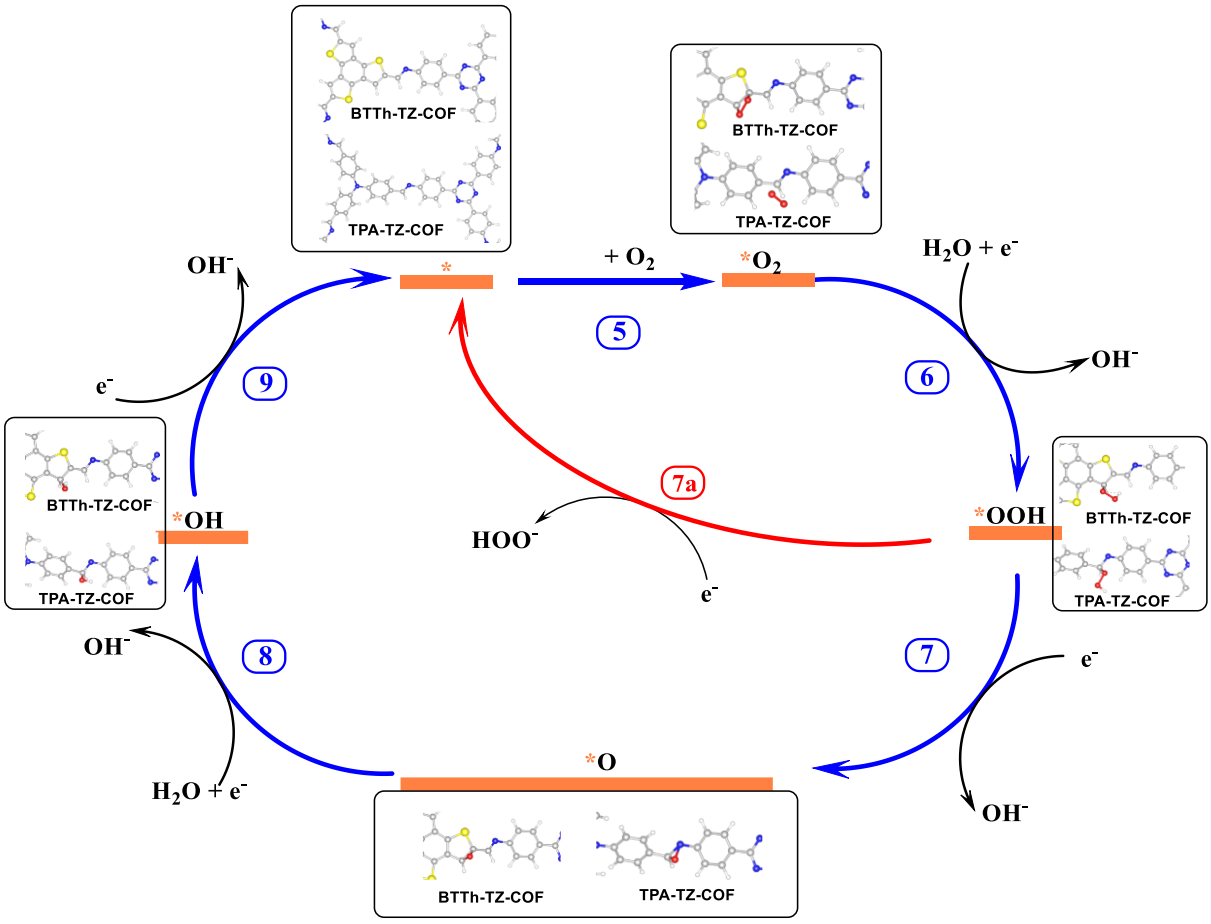

Fig. S17 Oxygen Reduction Reaction Mechanism on **BTTh-TZ-COF** and **TPA-TZ-COF**.

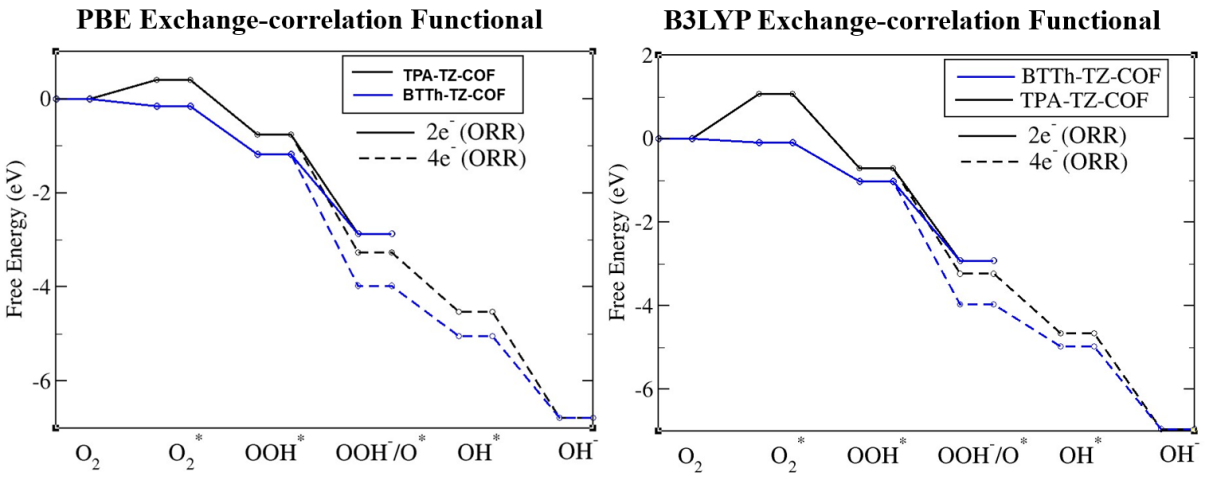

Fig. S18 The free energy diagram of ORR for **TPA-TZ-COF** (black) and **BTTh-TZ-COF** (blue). The dotted line represents the $4e^-$ mechanism while the solid line represents the $2e^-$ mechanism of ORR (See Eqn. 5-9) using PBE and B3LYP exchange-correlation functional.

Table S6. List of ZAB performance of COF-based materials.

Catalysts	OCV (V vs. RHE)	Areal Power Density (mW cm^{-2})	Specific Capacity (mAh)	Electrolyte	References
TAPP-Co-COF	1.34	103.73	750.51	Solution	21
JUC-650	1.38	101.5	722.6	Solution	12
TPDAB-Co@CNTs	1.46	156	_	Solution	22
CC-3	1.47	85	714	Solution	10
Pd@WTA-COF	1.52	189.7	770	Solution	23
Co-PorBpy-Co	1.45	159.4	_	Solution	24
PP/3D-NG	_	69.9	807	Solution	25
TAM-Tp	_	111.6	_	Solution	26
DPPS-COF	1.54	158.2	763.7	Solution	27
BTTh-TZ-COF	**1.13**	**26.36**	**23.84**	**Solid-State**	**This Work**
TPA-TZ-COF	**1.07**	**25.02**	**21.38**	**Solid-State**	**This Work**

References:

1. H. Liu, X. Zheng, J. Xu, X. Jia, M. Chao, D. Wang, and Y. Zhao, *ACS Appl. Mater. Interfaces,* 2023, *15*(13), 16794-16800.
2. S. Dalapati, M. Addicoat, S. Jin, T. Sakurai, J. Gao, H. Xu, S. Irle, S. Seki, D. Jiang, Nat. Commun., 2015, 6, 7786.

3. S. Ruidas, A. Das, S. Kumar, S. Dalapati, U. Manna, A. Bhaumik, Angew. Chem. Int. Ed., 2022, 61, e202210507.
4. J. Li, P. Liu, J. Mao, J. Yan, W. Song, *Nanoscale* **2022**, 14, 6126.
5. X.-F. Qiu, J.-R. Huang, C. Yu, Z.-H. Zhao, H.-L. Zhu, Z. Ke, P.-Q. Liao, X.-M. Chen, *Angew. Chem. Int. Ed.* **2022**, 61, e202206470.
6. L. Wang, C. Zeng, H. Xu, P. Yin, D. Chen, J. Deng, M. Li, N. Zheng, C. Gu, Y. Ma, *Chem. Sci.* **2019**, 10, 1023.
7. R. Zhao, T. Wang, J. Li, Y. Shi, M. Hou, Y. Yang, Z. Zhang, S. Lei, *Nano Res.* **2023**, 16, 8570.
8. S. Bhunia, A. Peña-Duarte, H. Li, H. Li, M. F. Sanad, P. Saha, M. A. Addicoat, K. Sasaki, T. A. Strom, M. J. Yacamán, C. R. Cabrera, R. Seshadri, S. Bhattacharya, J.-L. Brédas, L. Echegoyen, *ACS Nano* **2023**, 17, 3492.
9. S. Wei, F. Zhang, W. Zhang, P. Qiang, K. Yu, X. Fu, D. Wu, S. Bi, F. Zhang, *J. Am. Chem. Soc.* **2019**, 141, 14272.
10. S. S. A. Shah, M. S. Javed, T. Najam, M. A. Nazir, A. ur Rehman, A. Rauf, M. Sohail, F. Verpoort, S.-J. Bao, *Mater. Today* **2023**, 67, 229.
11. R. Cheng, B. Ran, X. Zhang, Y. Han, X. Shao, H. Li, and C. Fu, *Adv. Funct. Mater.*, 2024, *34*(42), 2406717.
12. R. Yang, S. Liu, Q. Sun, Q. Liao, K. Xi, B. Su, *J. Am. Chem. Soc.* **2022**, 144, 11778.
13. X.-Y. Dong, J.-J. Li, Z. Han, P.-G. Duan, L.-K. Li, S.-Q. Zang, *J. Mater. Chem. A* **2017**, 5, 3464.
14. G. S. Sauer, S. Lin, *ACS Catal.* **2018**, 8, 5175.
15. G. Kresse and J. Hafner, *Phys. Rev. B*, 47, **1993**, 558.
16. J. P. Perdew, K. Burke and M. Ernzerhof, *Phys. Rev. Lett.*, 1996, **77**, 3865
17. S. Grimme, S. Ehrlich, L. Goerigk, *J. Comput. Chem*., 32, **2011**, 1456-1465.
18. H. J. Monkhorst and J. D. Pack, *Phys. Rev. B,* 13, **1976**, 5188.
19. Nørskov, J. Kehlet, et al., *J. Phys. Chem. B,* 108, **2004**, 17886-17892.
20. Ma, R., Lin, G., Zhou, Y. et al., *NPJ Comput. Mater.,* 5, **2019**, 78.
21. X. Liang, Z. Zhao, R. Shi, L. Yang, B. Zhao, H. Qiao and L. Zhai, Molecules, 2023, 28, 4680.
22. J. Liu, T. Cheng, L. Jiang, H. Zhang, Y. Shan and A. Kong, Electro chim. Acta, 2020, 363, 137280.
23. W. Wang, L. Zhang, T. Wang, Z. Zhang, X. Wang, C. Cheng and X. Liu, J. Energy Chem., 2023, 77, 543–552.
24. J. Li, P. Liu, J. Yan, H. Huang and W. Song, Adv. Sci., 2023, 10, 2206165.
25. Y. Sun, P. Sun, J. Wang, Y. Zhuang, Y. Wu and Z. Li, J. Colloid Interface Sci., 2025, 686, 711–721.
26. Z. Mei, H. Li, G. Wang, Y. Mao, Y. Xu, J. Guo, Q. Li, H. Li, W. Li, Y. Tang and X. Liang, Appl. Surf. Sci., 2023, 615, 156324.

27. C. Lin, X. Yang, L. Zhai, S. An, H. Ma, Y. Fu, D. Han, Q. Xu and N. Huang, Small, 2024, 20, 2308143.